Analytical Prototypes for Ocean–Atmosphere Interaction at Midlatitudes. Part II: Mechanisms for Coupled Gyre Modes*

WENJIE WENG

Department of Atmospheric Sciences, University of California, Los Angeles, Los Angeles, California

J. DAVID NEELIN

Department of Atmospheric Sciences, and Institute of Geophysics and Planetary Physics, University of California, Los Angeles, Los Angeles, California

(Manuscript received 24 July 1998, in final form 4 November 1998)

ABSTRACT

A simple midlatitude coupled model for idealized ocean basins is used to investigate processes of ocean–atmosphere interaction and its role in interdecadal climate variability at midlatitudes. The ocean model consists of a linearized quasigeostrophic upper ocean layer and a sea surface temperature (SST) equation for an embedded surface mixed layer. The atmospheric response to the ocean is through wind stress and heat flux feedbacks associated with SST. Eigenvalue analysis of both coupled and uncoupled models presented here complements previous work on the stochastically forced system. Comparison of the eigenspectrum of coupled and uncoupled cases shows that coupling creates an oscillatory interdecadal mode whose properties are distinct from any other mode in the system. This mode exists whether the atmospheric feedbacks are weak or strong, and is stable even in the strong feedback case. The weak decay rate makes it possible for the mode to be maintained by atmospheric stochastic forcing. Analytic approximations to the dispersion relation show how the spatial structure of the atmospheric feedback tends to select a large-scale spatial pattern for this eigenmode. The oscillation involves westward Rossby wave propagation in the ocean with the atmosphere carrying information back eastward into the interior of the basin in response to SST anomalies produced by advection. SST modes are also found, which purely decay in most cases due to both local and nonlocal negative heat flux feedbacks. A case with large positive heat flux feedback can produce a purely growing SST mode but does not greatly impact the interdecadal mode.

1. Introduction

Large-scale spatial patterns of climate variability with interdecadal timescales have been noted over the North Atlantic and North Pacific Oceans (Folland and Parker 1989; Trenberth 1990; Wallace et al. 1990; Deser and Blackmon 1993). The source of such variability has been a subject of interest [see Latif (1998) for review]. The ''null hypothesis'' is that the upper ocean can integrate atmospheric white noise stochastic heat flux forcing to produce a red noise SST spectrum through its larger heat capacity (Hasselmann 1976; Frankignoul and Hasselmann 1977; Battisti et al. 1995). Other sources include teleconnections from the Tropics (e.g., Graham 1994; Trenberth and Hurrell 1994), internal ocean variability (e.g., Weaver et al. 1991, 1994; Chen and Ghil 1995; Spall 1996), and more complex response to atmospheric variability (e.g., Delworth et al. 1993; Saravanan and McWilliams 1997 and references therein).

In the study of the role of the atmospheric component in such variability, atmospheric general circulation model (GCM) experiments suggest that the midlatitude response to SST is modest compared to atmospheric internal variability, may have complex seasonal and nonlinear dependencies, and varies among models (Palmer and Sun 1985; Kushnir and Lau 1992; Ferranti et al. 1994; Peng et al. 1995). The question has been raised whether ocean–atmosphere interaction plays a role in at least some aspects of this climate variability (Bjerknes 1962; Namias and Cayan 1981; Kushnir 1994). Recent studies show that coupled GCMs can produce large-scale interdecadal oscillations (e.g., von Storch 1994; Latif and Barnett 1994, 1996; Robertson 1996; Zorita and Frankignoul 1997; Grötzner et al. 1998), in which atmospheric feedbacks appear to play a role. In the North Atlantic, an oscillation with an 18-yr period is reported by Grötzner et al. (1998) in two MPIM coupled models and Selten et al. (1999) find a 16–18-yr spectral

* UCLA-IGPP Paper Number 5102.

Corresponding author address: Dr. J. David Neelin, Department of Atmospheric Sciences, UCLA, Los Angeles, CA 90095-1565.
E-mail: neelin@atmos.ucla.edu

peak in their coupled model. Latif and Barnett (1994, 1996) and Robertson (1996) find timescales on the order of 20 yr in the North Pacific. However, the physical processes governing these timescales are still not clear.

Recently, several simple models have been presented to investigate the physical mechanisms governing the time and spatial scales of midlatitude interdecadal variability [Liu 1993; Jin 1997; Münnich et al. 1998; Neelin and Weng 1999 (NW99, hereafter); Weng and Neelin 1998 (WN98, hereafter)]. Jin (1997) suggests that this variability arises from the dynamic coupling and the memory of the system, residing in the slow gyre circulation adjustment. The important role of Rossby wave dynamics in the interdecadal mode is proposed by Münnich et al. (1998), NW99, and WN98. NW99 and WN98 further point out that the length scale of zonal wind stress also plays a crucial role in selecting the time and spatial scales of the mode.

In part I of this paper (NW99), an atmospheric model composed of atmospheric stochastic and SST-dependent noise processes is coupled to a shallow water ocean and a mixed layer SST equation. The results indicate that large-scale atmospheric stochastic forcing can produce a coherent spatial pattern and sometimes even a weak peak in the power spectrum at interdecadal timescale periods in the oceanic response (see also Frankignoul et al. 1997). Atmospheric feedback, although weak compared with atmospheric internal variability, can produce a significant impact on spatial patterns of SST anomalies and enhance the power spectral peak. This holds also in the limit that atmospheric SST-dependent noise approaches a deterministic feedback. The large-scale interdecadal mode has some features resembling oceanic Rossby wave dynamics, such as westward propagation. NW99 suggested that despite difficulties in distinguishing coupled variability from uncoupled, an atmospheric feedback combined with oceanic Rossby wave dynamics can play a significant role in the large-scale interdecadal climate variability at midlatitudes.

In Part II of this paper, we examine the eigenvalue problem to complement the time-marched modeling approach of Part I. We also seek a near-analytic solution of the coupled system to gain some insight into the role of coupling in generating the interdecadal oscillations. In particular, we examine how the interaction sets the time- and spatial scales of the motion and the role of heat flux and wind stress feedbacks. Section 2 gives a brief summary of the simple coupled model. Section 3 solves the eigenvalue problem for the coupled model. The results of the coupled and uncoupled modes for the North Atlantic and North Pacific Oceans are presented in sections 4 and 5. The physical mechanism of the interdecadal variability in both oceans is discussed in section 6 by seeking a near-analytic expression for frequency. A summary is given in section 7.

2. Model summary

We consider a linearized perturbation system with quasigeostrophic shallow water upper-ocean dynamics and an SST equation for a surface mixed layer. Both the vorticity and SST equations are written on a β-plane from 20°N to 60°N and are linearized about a basic state of rest. They are

$$\partial_t(\nabla^2 - \lambda^{-2})\psi_g + \beta\partial_x\psi_g = -\epsilon_c\nabla^2\psi_g + \nu\nabla^4\psi_g - \frac{\partial_y\tau_x}{\rho H} \tag{2.1}$$

$$\partial_t T = -\epsilon_T T + (\partial_x\overline{T}\partial_y - \partial_y\overline{T}\partial_x)\psi_g + \frac{\tau_x}{f\rho H_1}\partial_y\overline{T} + \frac{Q}{c_w\rho H_1}, \tag{2.2}$$

where $\nabla^2 = \partial_x^2 + \partial_y^2$, β is the latitudinal derivative of the Coriolis parameter (fixed at the 40°N value), and ψ_g is the perturbation geostrophic streamfunction. Here $\lambda\ (=c_0/f = \sqrt{g^*H}/f)$ is the Rossby deformation radius. The mean depth of the upper layer, H, is assumed to be 100 m; g^* is the reduced gravity and is chosen to give a wave speed c_0 about 3 m s^{-1}; and f is the Coriolis parameter at 40°N. These give a Rossby deformation radius of about 32 km. For damping terms in the vorticity equation, we include a Rayleigh damping applied to ocean current of rate ϵ_c, for which we test values between 0 and 1 yr^{-1}, and a horizontal turbulent viscosity coefficient, ν, with values in the range 10 m^2 s^{-1} to 10^4 m^2 s^{-1} (Pedlosky 1987). The effect of uncertainty associated with the values of ϵ_c and ν will be examined. Here τ_x is the zonal component of wind stress at the sea surface. The meridional component of wind stress is neglected. Here, T is the perturbation SST; $\overline{T}$ the climatological SST; ρ the seawater density; H_1 the depth of surface mixed layer, here 50 m; c_w the specific heat of seawater; ϵ_T the decay rate of SST anomaly due to local surface heat flux effects, here 2.73 yr^{-1}, estimated from Hamburg ECHAM-2 T21 GCM surface heat fluxes; and Q is the nonlocal heat flux at sea surface. Basic state currents are neglected in order to focus on processes arising from interaction with the atmosphere, rather than gyre instabilities.

The ocean model is coupled to the atmosphere through atmospheric wind stress and heat flux feedbacks associated with an SST basis function, θ_1. The spatial patterns of wind stress feedback, heat flux feedback, and the SST basis function are estimated based on atmospheric GCM results (see NW99 for detailed description). Wind stress patterns are simplified to aid analytical solution, while heat flux can be handled for any spatial pattern. We use the form

$$\tau_x = \mu\tau_A \cos(kx + \alpha)\cos(ly + \gamma)\langle\theta_1 T\rangle, \tag{2.3}$$

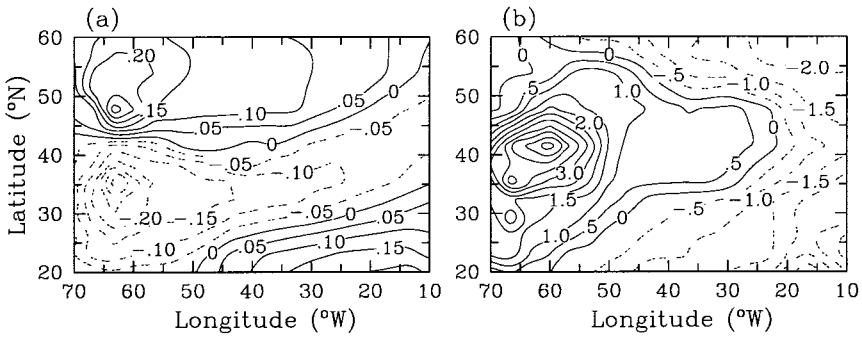

FIG. 1. (a) The estimate of the first SST basis function (contour interval 0.05 K), and (b) the estimate of heat flux feedback (contour interval 0.5 W m^{-2}) over the North Atlantic rectangular basin.

$$Q = \mu Q_{\rm fb}(x, y)\langle\theta_1 T\rangle, \tag{2.4}$$

where θ_1 is normalized by $\langle\theta_1^2\rangle$. Here τ_A is the amplitude, k the zonal wavenumber, l the meridional wavenumber, α and γ the phases, and μ a coupling coefficient for sensitivity studies. The western boundary is set at $x = 0$. The projection of SST on θ_1 over the basin is written $\langle\theta_1 T\rangle$ and $Q_{\rm fb}$ is a nonlocal heat flux feedback that is a function of space. In the North Atlantic, $\tau_A = 0.05$ dyn cm^{-2}, $k = 3/[R\cos(40°)]$, $l = 6/R$, $\alpha = 0.5\pi$, $\gamma = -0.8\pi$, where R is the radius of earth. The first SST basis function has an approximate north–south dipole pattern with a negative and a positive SST anomaly, centered near 30°N and 50°N, respectively. Both centers have maximum anomalies in the western Atlantic and extend toward the eastern Atlantic coastline. The nonlocal heat flux feedback shows large positive anomalies over most of the western North Atlantic, decreasing toward the east. These parameters and the fields θ_1 and $Q_{\rm fb}$ are estimated based on results from the Max-Planck Institut für Meteorologie's (MPIM) ECHAM-2 T21 atmospheric GCM, in an analysis similar to Graham et al. (1994), Zorita et al. (1992), and Kharin (1995) (see NW99 for detailed description). Figure 1 gives the estimated SST basis function, θ_1, and the nonlocal heat flux feedback for the idealized North Atlantic Ocean basin (as in WN98). These two fields are obtained by aligning the western boundary at the same longitude, and stretching the fields from the realistic basin accordingly. In the North Pacific, a crude estimation gives $\tau_A = 0.2$ dyn cm^{-2}, $\alpha = 0.075\pi$, $\gamma = -0.325\pi$, $2\pi/k$ about 13 600 km, and $2\pi/l$ about 8900 km for the Lau and Nath (1990) case. For the Latif and Barnett (1994) case, $\tau_A = 2$ dyn cm^{-2}, $\alpha = 0.375\pi$, $\gamma = -0.67\pi$, $2\pi/k$ is about 13 600 km, and $2\pi/l$ about 6700 km. The spatial patterns of the SST basis function and the nonlocal heat flux feedback are the same as those given in NW99 (Figs. 4 and 5 in NW99). Note here that we use $Q_{\rm fb}$ to represent the nonlocal heat flux feedback instead of Q_{s1} as used in NW99. Seasonal dependence may be important, but is neglected here for simplicity.

We note an implicit assumption that the atmospheric spatial pattern is set in the atmosphere, rather than as a coupled process. This is reasonable, given the preferred length scales that occur in atmospheric stationary wave dynamics. While we do not address the complex processes by which the pattern is set, we can follow through the consequences of any given atmospheric response pattern for the coupled system.

Equations (2.1)–(2.4) form ocean–atmosphere coupled model, which is the limit of the coupled model given in Part I of this paper (NW99) in which all standard deviations of atmospheric stochastic forcing go to zero. Here we carry out eigenvalue analysis of the deterministic coupled model both numerically and analytically. From this study, we shall provide physical mechanisms responsible for selecting both time- and spatial scales of the interdecadal mode.

3. Eigenvalue problem for the coupled model

To look for eigenmodes of the coupled system given in section 2, we assume that the time dependence of the geostrophic streamfunction, ψ_g, and the temperature anomaly, T, is separable from other variables, and has the form $e^{\sigma t}$. With the wind stress form given in (2.3), the dependence of ψ_g on y can be separated from other variables associated with feedbacks and is simply $\sin(ly + \gamma)$. That is, we look for solutions having the following form:

$$\psi_g(x, y, t) = e^{\sigma t}\tilde{\psi}(x)\sin(ly + \gamma) \tag{3.1}$$

$$T(x, y, t) = e^{\sigma t}\tilde{T}(x, y), \tag{3.2}$$

where σ is the frequency and $\tilde{T}(x, y)$ the spatial pattern of the SST anomaly.

From Eqs. (2.1)–(2.4) and (3.1)–(3.2), we obtain the Fourier transformed quasigeostrophic potential vorticity and SST anomaly equations

$$[\sigma(\partial_x^2 - l^2 - \lambda^{-2}) + \beta\partial_x + \epsilon_c(\partial_x^2 - l^2) - \nu(\partial_x^2 - l^2)^2]\tilde{\psi}(x) = \frac{\mu l \tau_A}{\rho H}\cos(kx + \alpha)\langle\theta_1\tilde{T}\rangle \quad (3.3)$$

$$(\sigma + \epsilon_T)\tilde{T}(x, y) = [l\cos(ly + \gamma)\partial_x\overline{T} - \sin(ly + \gamma)\partial_y\overline{T}\partial_x]\tilde{\psi}(x) + \left[\frac{\mu\tau_A}{f\rho H_1}\cos(kx + \alpha)\cos(ly + \gamma)\partial_y\overline{T} + \frac{\mu Q_{\text{fb}}}{c_w\rho H_1}\right]\langle\theta_1\tilde{T}\rangle. \quad (3.4)$$

Since the inner product of θ_1 and $\tilde{T}$ is constant over the basin, the vorticity Eq. (3.3) becomes one-dimensional. When $\mu \neq 0$, (3.3) and (3.4) form the eigensystem of the coupled model. When $\mu = 0$, it becomes an uncoupled ocean-only model. We carry forward the analytic solution for ocean variables, given the frequency and the atmospheric feedback patterns in sections 3a and 3b, and derive the corresponding frequency equation in section 3c. The spatial patterns of sections 3a and 3b also provide the eigenvectors once the frequency is known.

a. Solution of the potential vorticity equation

For a given frequency, Eq. (3.3) has a particular solution:

$$\psi_P(x) = -\frac{\mu l \tau_A\langle\theta_1\tilde{T}\rangle}{\rho H(A^2 + \beta^2k^2)} \times [A\cos(kx + \alpha) - \beta k\sin(kx + \alpha)], \quad (3.5)$$

where

$$A = \sigma\Lambda^{-2} + \epsilon_c K^2 + \nu K^4 \quad (3.6)$$

$$K^2 = k^2 + l^2 \quad (3.7)$$

$$\Lambda^{-2} = k^2 + l^2 + \lambda^{-2}. \quad (3.8)$$

To obtain this particular solution, we have assumed that frequency is such that $A^2 + \beta^2k^2 \neq 0$. We show in section 3c that for the coupled system (i.e., $\mu \neq 0$), this assumption is generally satisfied (although the departures from zero may be small). This particular solution has the same sinusoid form as the wind stress feedback in zonal direction, but there is a phase shift between these two, and this shift depends on frequency.

Since both zonal and meridional wavelengths of the wind stress feedback are much larger than the deformation radius at midlatitude, Λ in (3.8) is determined by the Rossby deformation radius and is about 32 km in both the North Atlantic and North Pacific Oceans.

Let

$$\tilde{\psi}(x) = \psi_H(x) + \psi_P(x). \quad (3.9)$$

The homogeneous solution $\psi_H(x)$ satisfies Eq. (3.3) separately,

$$[\sigma(\partial_x^2 - l^2 - \lambda^{-2}) + \beta\partial_x + \epsilon_c(\partial_x^2 - l^2) - \nu(\partial_x^2 - l^2)^2]\psi_H(x) = 0 \quad (3.10)$$

and can be written as

$$\psi_H(x) = \frac{\mu l \tau_A\langle\theta_1\tilde{T}\rangle}{\rho H(A^2 + \beta^2k^2)}\psi_h(x, \sigma), \quad (3.11)$$

where $\psi_h(x, \sigma)$ is given by Eq. (A.4) in appendix A. In solving the homogeneous solution, we have used no normal flow and no-slip boundary conditions.

From (3.5), (3.9), and (3.11), the solution for $\tilde{\psi}(x)$ is

$$\tilde{\psi}(x) = \frac{\mu l \tau_A\langle\theta_1\tilde{T}\rangle}{\rho H(A^2 + \beta^2k^2)} \times [\beta k\sin(kx + \alpha) - A\cos(kx + \alpha) + \psi_h(x, \sigma)], \quad (3.12)$$

where A is given by (3.6) and $\psi_h(x, \sigma)$ is given by (A.4) with appropriate values of r_i and c_i ($i = 1, 2, 3, 4$) for $\nu = 0$ or $\nu \neq 0$. The above expression shows that the zonal component of the wind stress feedback pattern plays a role in geostrophic streamfunction, but the shape of $\tilde{\psi}(x)$ across the basin is not yet clear due to the unknown frequency and the complicated expression for the homogeneous solution.

b. Solution of the SST equation

Substituting the solution of $\tilde{\psi}(x)$ for a given frequency from (3.12) into the SST Eq. (3.4), we obtain

$$(\sigma + \epsilon_T)\tilde{T}(x, y) = \mu\left\{\frac{l\tau_A}{\rho H(A^2 + \beta^2k^2)}\mathcal{L}[\beta k\sin(kx + \alpha) - A\cos(kx + \alpha) + \psi_h(x)] + \frac{\tau_A}{f\rho H_1}\cos(kx + \alpha)\cos(ly + \gamma)\partial_y\overline{T} + \frac{Q_{\text{fb}}}{c_w\rho H_1}\right\}\langle\theta_1\tilde{T}\rangle, \quad (3.13)$$

where the operator $\mathcal{L}$ is defined by

$$\mathcal{L} = l\cos(ly + \gamma)\partial_x\overline{T} - \sin(ly + \gamma)\partial_y\overline{T}\partial_x. \quad (3.14)$$

Let

$$Q_{\mathrm{FB}}(x, y) = \frac{Q_{\mathrm{fb}}(x, y)}{c_w\rho H_1} \quad (3.15)$$

$$V_E(x, y) = \frac{\tau_A}{f\rho H_1}\cos(kx + \alpha)\cos(ly + \gamma)\partial_y\overline{T} \quad (3.16)$$

$$V_P(x, y) = -\frac{l\tau_A}{\rho H}\mathcal{L}[e^{i(kx+\alpha)}] \quad (3.17)$$

$$V_H(x, y, \sigma) = \frac{l\tau_A}{i\beta k\rho H}\mathcal{L}[\psi_h(x, \sigma)], \quad (3.18)$$

where $Q_{\mathrm{FB}}(x, y)$ is the heat flux feedback normalized by heat capacity, and V_E is the advection of climatological SST by Ekman current. The quantities V_P and V_H are related to the advection of climatological SST by the geostrophic current produced by shallow water wave motion with certain boundary conditions. With these definitions (3.15)–(3.18), the solution for $\tilde{T}(x, y, \sigma)$ is

$$\tilde{T}(x, y, \sigma) = \left\{\frac{i\beta kV_H(x, y, \sigma) + A(\sigma)\mathrm{Re}(V_P(x, y)) - \beta k\mathrm{Im}(V_P(x, y))}{A^2(\sigma) + \beta^2k^2} + Q_{\mathrm{FB}}(x, y) + V_E(x, y)\right\}\frac{\mu\langle\theta_1\tilde{T}\rangle}{\sigma + \epsilon_T}, \quad (3.19)$$

where $\mathrm{Re}(V_P)$ and $\mathrm{Im}(V_P)$ are the real and imaginary parts of V_P, respectively, and $A(\sigma)$ is given by (3.6).

From (3.19), the spatial pattern of the SST anomaly is determined by the nonlocal heat flux feedback and the advection of climatological SST by geostrophic and Ekman currents. Frequency plays an important role in choosing the term dominating the spatial pattern.

c. Frequency equation

In sections 3a and 3b, we find solutions of geostrophic streamfunction and SST anomalies for a given frequency. The remaining task is to find the frequency for this eigensystem. Taking the inner product of θ_1 with Eq. (3.19) over the basin, canceling $\langle\theta_1\,\tilde{T}\rangle$ from both sides, and rearranging it, we obtain

$$(\sigma + \epsilon_T - \mu\langle\theta_1Q_{\mathrm{FB}}\rangle - \mu\langle\theta_1V_E\rangle)[A^2(\sigma) + \beta^2k^2] = \mu[i\beta k\langle\theta_1V_H(\sigma)\rangle + A(\sigma)\langle\theta_1\mathrm{Re}(V_P)\rangle - \beta k\langle\theta_1\mathrm{Im}(V_P)\rangle]. \quad (3.20)$$

Since the spatial forms of the SST basis function and the atmospheric feedbacks are known, the inner products over the basin of θ_1 with Q_{FB}, V_P, and V_E, respectively, are known constants. The term $A(\sigma)$ is simply a first-order polynomial, and $\langle\theta_1V_H(\sigma)\rangle$ is a function of frequency only since V_H depends on x, y, and σ. Thus (3.20) has only one unknown, the frequency. Note that in this frequency equation, nonlocal effects, such as the heat flux feedback $Q_{\mathrm{FB}}(x, y)$ enter via the projection of the nonlocal heat flux feedback onto the SST basis function, $\langle\theta_1Q_{\mathrm{FB}}\rangle$. Therefore, the spatial patterns of both the feedbacks and the SST basis function play a role and provide an overall effect on frequency. The effect of the advection of climatological SST by ocean currents on frequency is treated similarly.

The right-hand side of Eq. (3.20) comes from the advection of climatological SST by geostrophic current. Usually it will not be zero when there is geostrophic current. Then $A^2(\sigma) + \beta^2k^2$ in (3.20) cannot be zero when μ is not zero. The assumption of $A^2 + \beta^2k^2 \neq 0$ for the coupled system is thus satisfied.

If we replace A in (3.20) by (3.6) and rearrange it, we obtain another form of frequency equation

$$\sigma^3 + b_1\sigma^2 + b_2\sigma + b_3 - b_H(\sigma) = 0, \quad (3.21)$$

where

$$b_1 = \epsilon_T - \mu(\langle\theta_1Q_{\mathrm{FB}}\rangle + \langle\theta_1V_E\rangle) + 2\Lambda^2(\epsilon_cK^2 + \nu K^4), \quad (3.22)$$

$$b_2 = \beta^2k^2\Lambda^4 - \mu\langle\theta_1\mathrm{Re}(V_P)\rangle\Lambda^2 + (\epsilon_cK^2 + \nu K^4)^2\Lambda^4 + 2[\epsilon_T - \mu(\langle\theta_1Q_{\mathrm{FB}}\rangle + \langle\theta_1V_E\rangle)] \times (\epsilon_cK^2 + \nu K^4)\Lambda^2, \quad (3.23)$$

$$b_3 = \beta^2k^2[\epsilon_T - \mu(\langle\theta_1Q_{\mathrm{FB}}\rangle + \langle\theta_1V_E\rangle)]\Lambda^4 + \mu\beta k\langle\theta_1\mathrm{Im}(V_P)\rangle\Lambda^4 - \mu(\epsilon_cK^2 + \nu K^4)\langle\theta_1\mathrm{Re}(V_P)\rangle\Lambda^4 + [\epsilon_T - \mu(\langle\theta_1Q_{\mathrm{FB}}\rangle + \langle\theta_1V_E\rangle)] \times (\epsilon_cK^2 + \nu K^4)^2\Lambda^4, \quad (3.24)$$

$$b_H(\sigma) = i\beta k\mu\langle\theta_1V_H(\sigma)\rangle\Lambda^4. \quad (3.25)$$

In b_1, b_2, b_3, and b_H, all the variables and parameters except frequency are given. Then b_1, b_2, and b_3 in Eq. (3.21) are known values and b_H is a function of frequency since $\langle\theta_1V_H\rangle$ depends on frequency. Because b_H has a complicated dependence on frequency, it is not straightforward to find an analytic solution to Eq. (3.21). It can be solved numerically by an iteration method, or further approximations can be made. Once the frequency is obtained, the eigenvectors of the streamfunction and

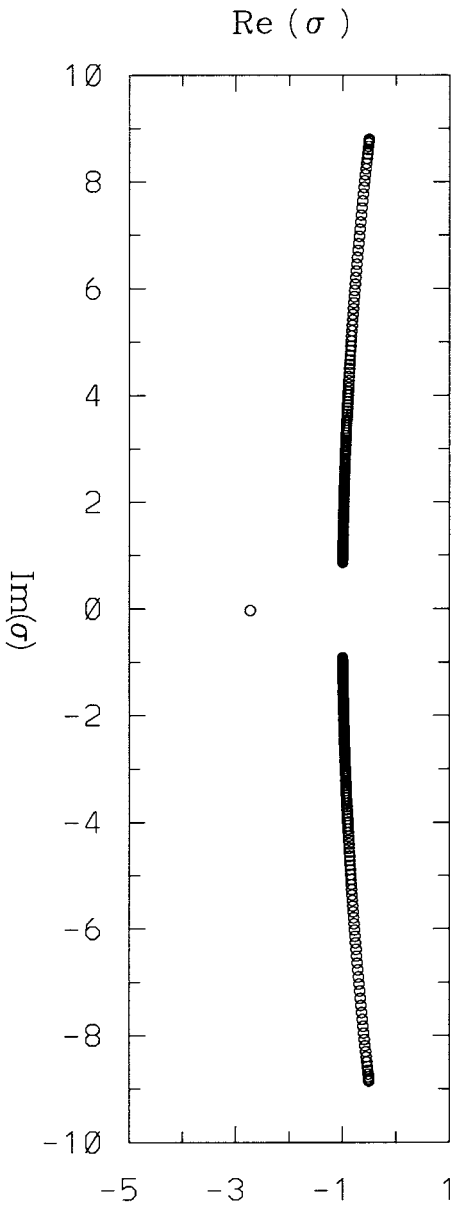

FIG. 2. The eigenvalues on the complex plane for the uncoupled case in the North Atlantic. There is a large set of ocean basin modes (shown for $n = 1, 3, 5, \ldots, 499$ for the case of $\epsilon_c = 1$ yr^{-1} and $\nu = 0$) that appear as an ''almost continuous'' spectrum. The separated eigenvalue is the SST mode. Frequency is in yr^{-1}.

SST anomalies are obtained analytically from (3.12) and (3.19), respectively.

4. Coupled eigenmodes versus uncoupled ocean spectrum

Solving the frequency equation (3.21) numerically, we compare the standard coupling case (that is, $\mu = 1$), with the eigenmodes for an uncoupled ocean-only model [$\mu = 0$ in Eqs. (3.3) and (3.4)]. Figure 2 shows the eigenvalues of the uncoupled modes on the complex plane for the North Atlantic case (see appendix B for details). One mode purely decays with a decay rate of about 2.73 yr^{-1}. We call this the SST mode since it is related to the time derivative of the SST equation. The decay rate of the SST mode is due to the local negative heat flux feedback. Strictly speaking this eigenvalue represents a degenerate set of modes, but this is not of interest here. Besides the SST mode, there is another set of modes—the ocean basin modes—with decay rates ranging from 0.5 to 1 yr^{-1}, and with periods of about 0.7 yr or longer. The frequencies of these modes are determined by the vorticity equation and the decay rates depend on the damping coefficients in the equation. In the figure shown here, we consider a simple case with $\nu = 0$. For $\epsilon_c = 1$ yr^{-1}, the gravest mode [$n = \pm 1$ in Eq. (B.3)] has the highest frequency of about 9 yr^{-1} and has a decay rate of 0.5 yr^{-1}. As analyzed in appendix B, the ocean basin modes have zonal length scales similar to the Rossby deformation radius (here about 32 km) or less. It is not expected that ocean basin modes are individually observable, since their eigenvalues are very close and they have complicated spatial structures. They are presented simply as background for considering the effects of coupling. We also note that inclusion of mean advection, $\overline{\mathbf{V}} \cdot \boldsymbol{\nabla}$ terms, in the model can significantly affect the modes of the system (e.g., Speich et al. 1995).

The SST mode and the ocean basin modes also exist in the coupled system ($\mu = 1$). The coupled ocean basin modes have decay rates and frequencies similar to that of the corresponding uncoupled modes (Fig. 3). For instance, the gravest coupled ocean basin mode [$n = \pm 1$ in (C.1)] has a decay rate of 0.5 yr^{-1} and a frequency of about 9 yr^{-1}, which is basically the same as that of the corresponding uncoupled mode. The eigenvectors of the coupled ocean basin modes are also similar to the corresponding uncoupled modes given in (B.6) and (B.7). Coupling has no significant influence on most of the ocean basin mode spectrum. The ocean basin modes are not our major concern since we are interested in large-scale wave motions. Like the uncoupled SST mode, the coupled SST mode decays purely but with a decay rate of 3.6 yr^{-1} (Fig. 3), which is larger than that of the uncoupled case. The increase of the decay rate is mainly due to the addition of the nonlocal negative heat flux feedback effect on the local heat flux feedback.

Besides the SST mode and the ocean basin modes, there is another type of coupled mode that is not found in the uncoupled model. This coupled mode has a period of 18 yr and a decay rate on the order of 10^{-2} yr^{-1} or less. We call it the interdecadal mode because of its interdecadal timescale. This is the most interesting mode due to its small decay rate, longer oscillation period, and large spatial scale. Analysis of the associated eigenvectors is given in the next section. The main point here is that this eigenvalue stands out distinctly from anything found in the uncoupled ocean spectrum. This eigenvalue is also very robust numerically, whereas oth-

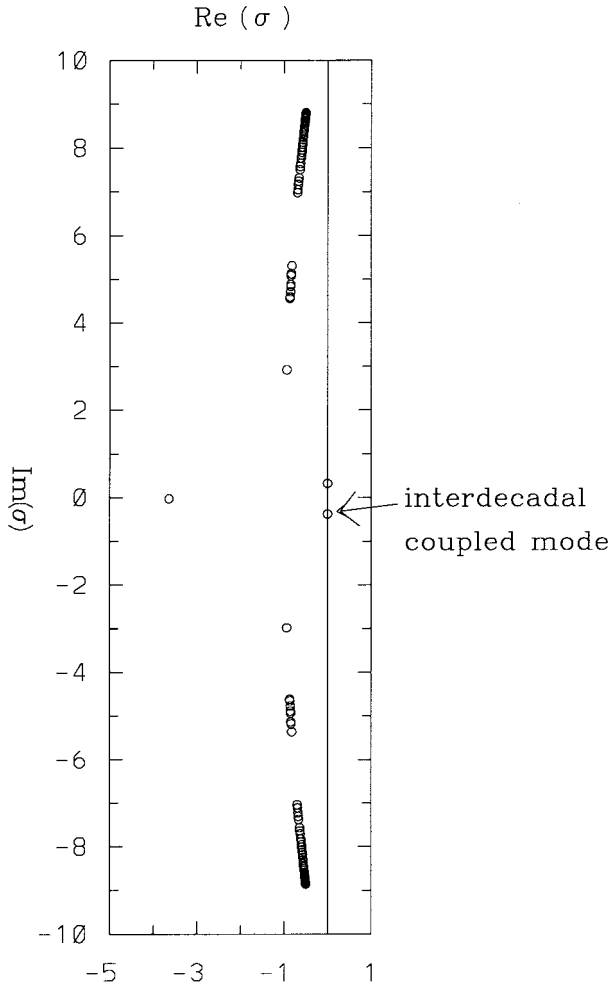

FIG. 3. The eigenvalues on the complex plane for the coupled case in the North Atlantic (for $\epsilon_c = 1$ yr^{-1}). Only 44 ocean basin mode eigenvalues are shown due to difficulties in numerical convergence. The SST mode eigenvalue is separated at strongly negative Re(σ). The weakly decaying (10^{-3} yr^{-1}), distinct eigenvalues of the interdecadal mode are produced by the effects of coupling. Frequency is in yr^{-1}.

er parts of the ocean spectrum can have numerical convergence problems associated with the near-degeneracy of the modes.

The uncoupled modes in the North Pacific are basically similar to the North Atlantic case, as can be seen from (B.1) and (B.3). For the coupled case, we examine the Lau and Nath (1990) case and the Latif and Barnett-like case. The Latif and Barnett-like case is defined as that with the magnitudes of heat flux and wind stress feedbacks reduced to the same magnitudes as estimated in the Lau and Nath (1990) case, but keeping the Latif and Barnett spatial feedback patterns and their positive heat flux feedback. The reason for this adjustment is given in NW99. Our investigation for these two cases shows that for both the effect of coupling is qualitatively similar to the North Atlantic case. The quantitative difference is that the period of the interdecadal mode is 24 yr, which is longer than that of the North Atlantic case. For the Lau and Nath case, the decay rate of the SST mode is about 4.29 yr^{-1}, which is larger than that of the uncoupled case. The Latif and Barnett-like case has a smaller decay rate of about 1.23 yr^{-1}. This is because of the negative heat flux feedback in the Lau and Nath (1990) case versus the positive heat flux feedback in the Latif and Barnett-like case.

5. Model solutions for North Atlantic and North Pacific cases

This section focuses on the eigenvectors of the coupled SST mode and the interdecadal mode since both of them have large-scale features. Figure 4 shows the spatial pattern of the SST anomaly and the zonal variation of the streamfunction in the North Atlantic for the SST mode. The similarity between Figs. 4a and 1b indicates the dominant role of the nonlocal heat flux feedback in generating the SST anomalies. The streamfunction is dominated by the wind stress feedback pattern. The SST mode decays purely, that is, the heat flux feedback does not produce an oscillatory mode in this model.

The eigenvector of the interdecadal mode for the North Atlantic case is given in Fig. 5. The spatial SST anomalies (Figs. 5a,c) have a north–south dipole pattern with maximum anomalies in the western Atlantic. The zonal structures of the geostrophic streamfunction (Figs. 5b,d) have smooth large-scale patterns that decay toward the east. These features are similar to those found by the time integration method in the stochastically forced case (NW99). The time–longitude dependence of the geostrophic streamfunction for this mode (Fig. 6a) shows westward propagation during the interdecadal oscillation. There is counterflow on the east side of the boundary current, due to balances involving the horizontal diffusion term in the vorticity equation. Note that the evolution of the SST anomalies (Fig. 6b) shows much less tendency to westward propagation than that of the streamfunction. The heat flux feedback contributes slightly to this difference, but the main effect is that the magnitude of $\nabla\overline{T}$ varies within the basin. The term $u_g\partial_x\overline{T}$ plays a significant role in the case shown.

Tests with ϵ_c ranging from 0 to 1 yr^{-1} and ν ranging from 0 to 10^4 m^2 s^{-1}, show that the decay rate of the SST mode, the period of the interdecadal mode, and the spatial patterns of both SST and interdecadal modes are not very sensitive to these coefficients. Essentially, the form of the damping influences only the western boundary layer, with the thickness of the layer increasing with the viscosity coefficient (Fig. 7). Both the friction and diffusion terms produce the decay rate in the interdecadal mode. For the above range of these two coefficients, the decay rate is on the order of 10^{-2} yr^{-1} or less. We note that without the friction term (i.e., $\epsilon_c = 0$), this mode still exists.

As in the North Atlantic case, the spatial SST anom-

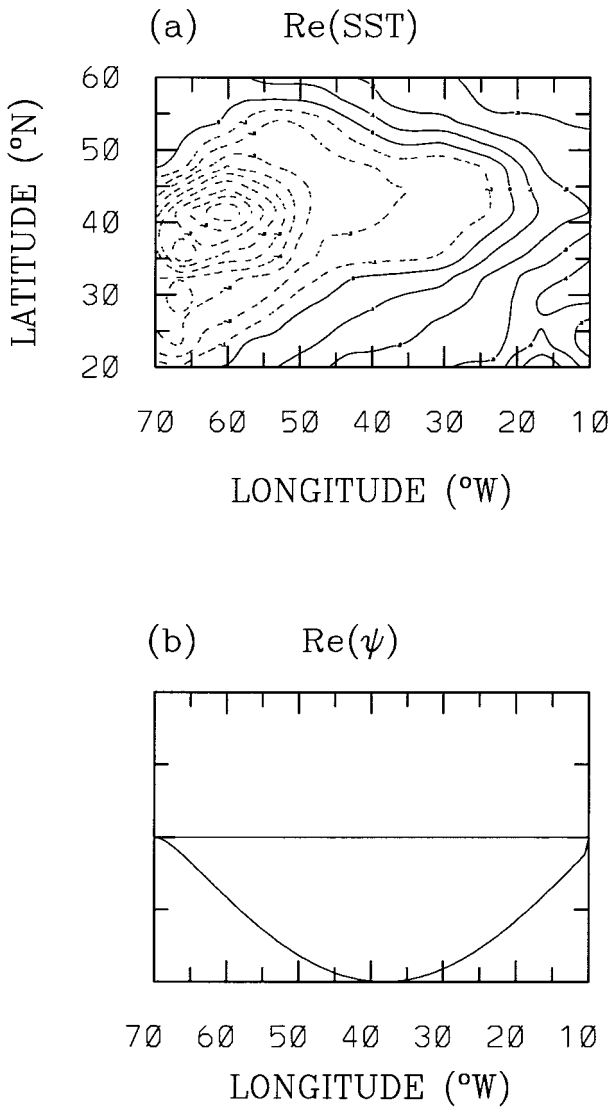

FIG. 4. The eigenvector of the SST mode in the North Atlantic. (a) The spatial distribution of the SST anomaly, and (b) the zonal dependence of the streamfunction. Imaginary parts are zero.

alies and the zonal component of the streamfunction of the purely decaying SST mode in the North Pacific are dominated by the nonlocal heat flux feedback and the wind stress feedback patterns, respectively (see Figs. 8 and 9). For comparison, the nonlocal heat flux feedback patterns for the Lau and Nath and Latif and Barnett cases are given in NW99. Although the spatial patterns of the heat flux and wind stress differ among Pacific and Atlantic cases, the underlying physical interpretation is the same.

The eigenvectors of the interdecadal mode for the Lau and Nath (1990) case and the Latif and Barnett-like case are shown in Figs. 10 and 11, respectively. Both cases have a period of 24 yr and a decay rate on the order of 10^{-2} yr^{-1} or less. Like the case in the North Atlantic, the SST anomalies have a north–south dipole pattern and the zonal structure of the geostrophic streamfunction has a smooth large-scale pattern, which decays eastward. This mode propagates toward the west and oscillates with time. Consistent with the results obtained in NW99, the period and the zonal length scale in the North Pacific are longer than that in the North Atlantic. We note that for either case, the eigenvalue and eigenvector of the interdecadal mode are qualitatively similar. This indicates that the interdecadal mode is fairly insensitive to the detailed features of the basis functions or feedback patterns, and is not very sensitive even to the sign of the heat flux feedback.

For the Latif and Barnett (1994) case, in which there are large heat flux and wind stress feedbacks, the SST mode has a positive growth rate of 7.7 yr^{-1}. The SST anomalies and streamfunction of the SST mode are similar to the case of Fig. 9, and are still dominated by the nonlocal heat flux and wind stress feedbacks, respectively. The interdecadal mode has the same period and spatial structures as that in the Latif and Barnett-like case (Fig. 11), indicating that the feedback magnitudes do not have significant influence on the interdecadal mode. Furthermore, the interdecadal mode is not unstable even for large positive heat flux feedback and strong wind stress feedback.

6. Analytic approximations to the eigenvalue problem

To better understand the physical mechanism of the large-scale coupled modes, especially the interdecadal mode, we look for a near-analytic solution of frequency. Because the term $\langle \theta_1 V_H(\sigma) \rangle$ in frequency Eq. (3.20) or (3.21) has a complicated dependence on frequency, involving both shape and coefficients, it is unlikely that an exact analytic solution can be obtained. Instead, we look for an approximate analytic expression for frequency, and from it, some insight into the dynamic process selecting the time and spatial scales of the large-scale motions in the coupled system.

For $\mu = 1$, ϵ_c between 0 and 1 yr^{-1}, and ν between 0 and 10^4 m^2 s^{-1}, the orders of magnitude of b_1, b_2, and b_3 are 10^0 yr^{-1}, $\leq 10^{-1}$ yr^{-2}, and 10^{-1} yr^{-3}, respectively, for the Atlantic case, the Lau and Nath (1990) case, and the Latif and Barnett-like case. Our numerical results show that b_H is of the order of 10^{-1} yr^{-3} or less for both the interdecadal and SST modes. We look for near-analytic solutions for the SST mode and interdecadal mode under these circumstances. By assuming b_H is known, the frequency equation (3.21) has three explicit analytic solutions for frequency. Using power series and scaling analysis [see Weng (1997) for detailed derivation], these solutions can be simplified to approximate expressions for the frequency for SST and interdecadal modes, respectively,

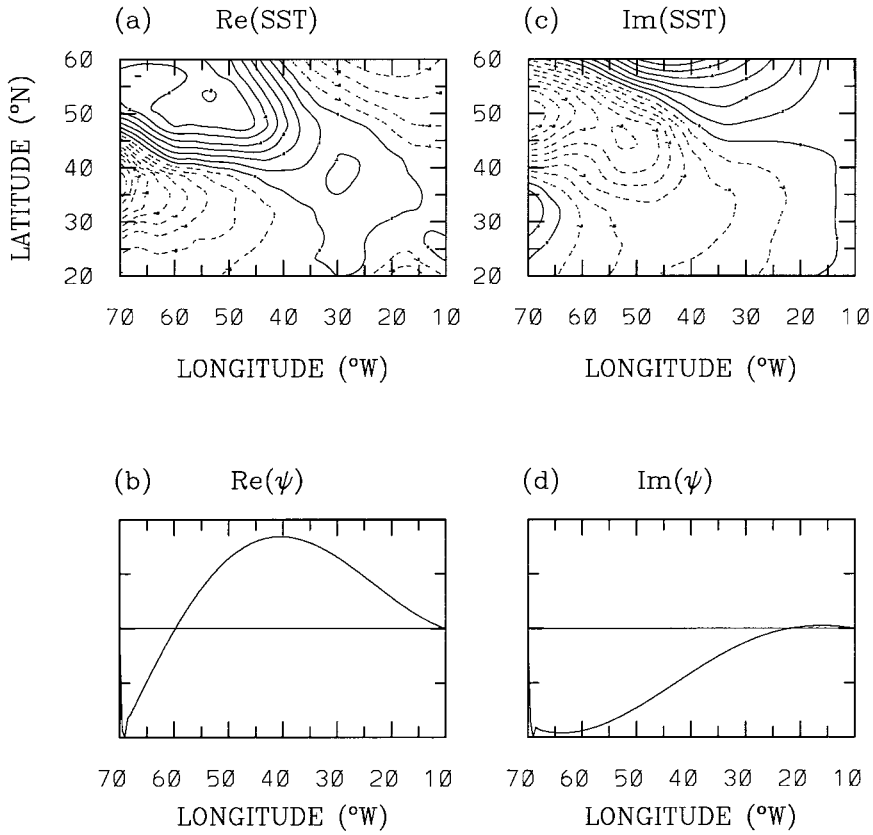

FIG. 5. The eigenvector of the interdecadal mode in the North Atlantic (for $\epsilon = 1$ yr^{-1} and $\nu = 100$ m^2 s^{-1}.) (a) The real part of $\tilde{T}(x, y)$, (b) the real part of $\tilde{\psi}(x)$, (c) the imaginary part of $\tilde{T}(x, y)$, (d) the imaginary part of $\tilde{\psi}(x)$.

$$\sigma_1 \approx -b_1 - \frac{b_3 - b_H - b_1 b_2}{b_1^2} \tag{6.1}$$

$$\sigma_{2,3} \approx \frac{b_3 - \mathrm{Re}(b_H) - b_1 b_2}{2b_1^2} \pm \frac{\mathrm{Im}(b_H)}{2b_1}\sqrt{\frac{b_1}{b_3 - \mathrm{Re}(b_H)}} \pm i\sqrt{\frac{b_3 - \mathrm{Re}(b_H)}{b_1}}, \tag{6.2}$$

where b_H is $b_H(\sigma_1)$ in (6.1) and $b_H(\sigma_{2,3})$ in (6.2).

a. The SST mode

From (6.1), the frequency of the SST mode is dominated by $-b_1$. We use $-b_1$ as the frequency to estimate b_H. With the aid of (3.22)–(3.25), (6.1) can be written as

$$\sigma_1 \approx -\underbrace{\epsilon_T}_{\text{term 1}} + \underbrace{\mu\langle\theta_1 Q_{\mathrm{FB}}\rangle}_{\text{term 2}} + \underbrace{\mu\langle\theta_1 V_E\rangle}_{\text{term 3}} - \underbrace{\frac{\mu\beta k\Lambda^4\langle\theta_1 \mathrm{Im}(V_P)\rangle - b_{H0}}{b_1^2}}_{\text{term 4}} - \underbrace{\frac{\mu\Lambda^2\langle\theta_1 \mathrm{Re}(V_P)\rangle}{b_1}}_{\text{term 5}} \tag{6.3}$$

where we omit terms whose dimensional order of magnitude is smaller than 10^{-2} year^{-1}. This approximate solution clearly shows that the effect of heat flux is to produce a nonoscillatory SST mode, consistent with the numerical results in section 4. Whether the nonlocal heat flux feedback causes the mode to decay or grow depends on the sign of $\langle\theta_1 Q_{\mathrm{FB}}\rangle$, and on its magnitude compared to ϵ_T.

TABLE 1. Estimate of various terms in Eq. (6.3) for the North Atlantic and North Pacific oceans when $\mu = 1$, $\epsilon_c = 1$ yr^{-1}, and $\nu = 0$.

	Term 1	Term 2	Term 3	Term 4	Term 5
Atlantic	2.73	−0.82	0.04	$\leq 10^{-3}$	−0.14
Lau and Nath case (1990)	2.73	−1.79	0.26	$\leq 10^{-3}$	$\leq 10^{-2}$
Latif and Barnett-like case	2.73	1.31	0.28	$\leq 10^{-2}$	0.1
Latif and Barnett case (1994)	2.73	7.65	2.67	$\leq 10^{-2}$	−0.13

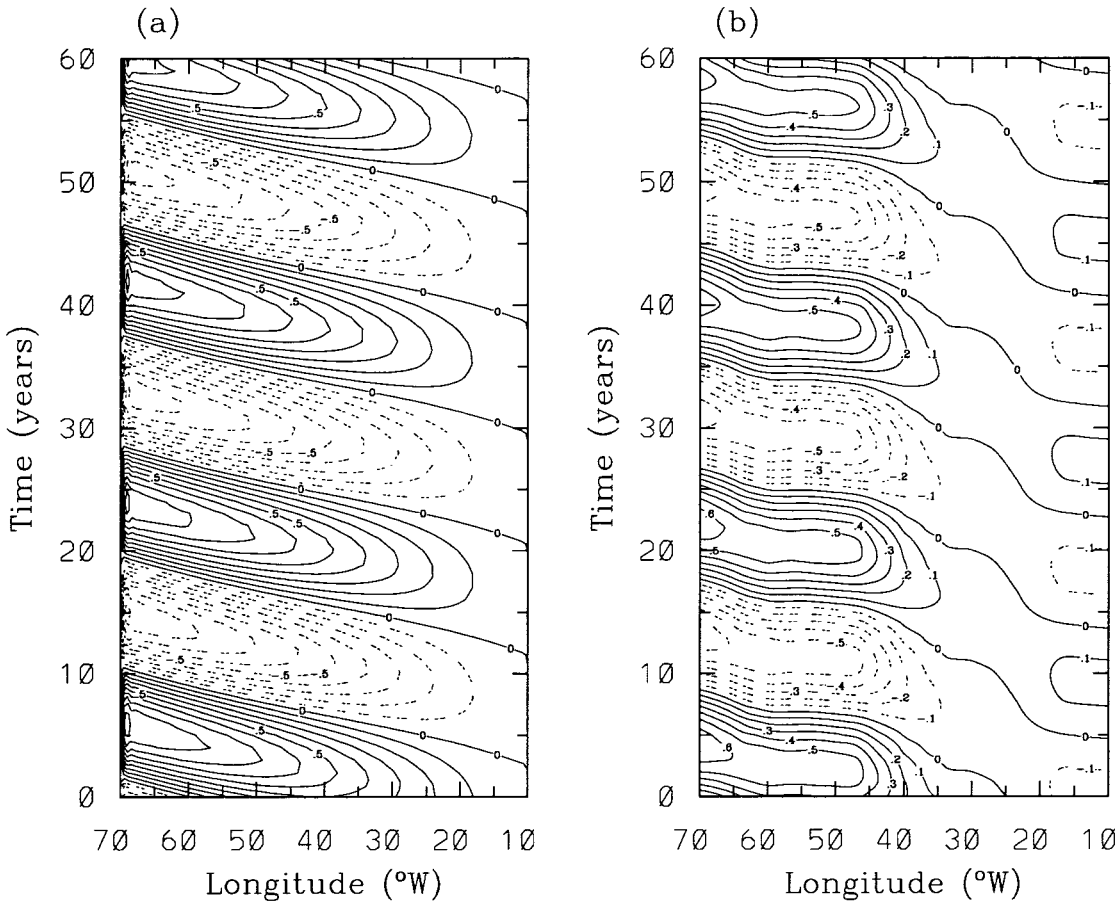

FIG. 6. The time–longitude dependence of (a) the geostrophic streamfunction, and (b) the SST anomalies at 50°N for the interdecadal mode in the North Atlantic when $\epsilon_c = 1$ yr^{-1} and $\nu = 100$ m^2 s^{-1}

When $\mu = 1$ and $\epsilon_c = 1$ yr^{-1}, (6.3) gives a decay rate of 3.65 yr^{-1} in the North Atlantic, and 4.3 and 1.2 yr^{-1} in the North Pacific for the Lau and Nath (1990) case and Latif and Barnett-like case, respectively. These decay rates are close to the numerical results obtained in section 4. Table 1 gives the values of the five terms in Eq. (6.3) for the standard coupling case. For all cases, the decay rate of the SST mode is mainly due to the local negative heat flux feedback (i.e., $-\epsilon_T$) and the nonlocal heat flux feedback (i.e., $\langle \theta_1 Q_{FB} \rangle$). The advection of climatological SST by geostrophic current plays a relatively small role in the SST mode. The Ekman current effects are small except in the Latif and Barnett case, where the strong wind stress feedback produces a substantial Ekman component that reinforces the positive heat flux feedback.

The approximate analytic expression for frequency given in (6.3) is obtained under the assumption that the atmospheric wind stress and heat flux feedbacks are

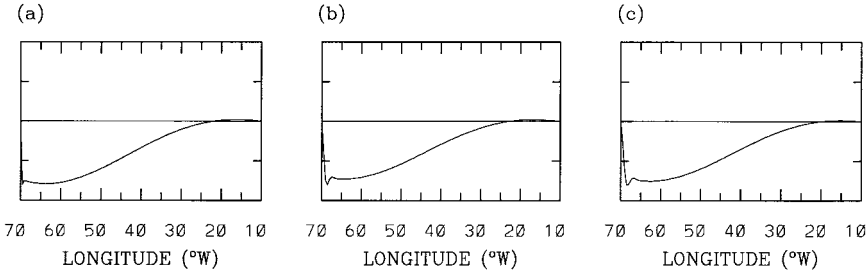

FIG. 7. The zonal structure of geostrophic streamfunction for one phase of the interdecadal mode in the North Atlantic for different values of viscosity ν. The phase shown in Fig. 5d is chosen for illustration: (a) $\nu = 10$ m^2 s^{-1}, (b) $\nu = 500$ m^2 s^{-1}, (c) $\nu = 1000$ m^2 s^{-1}.

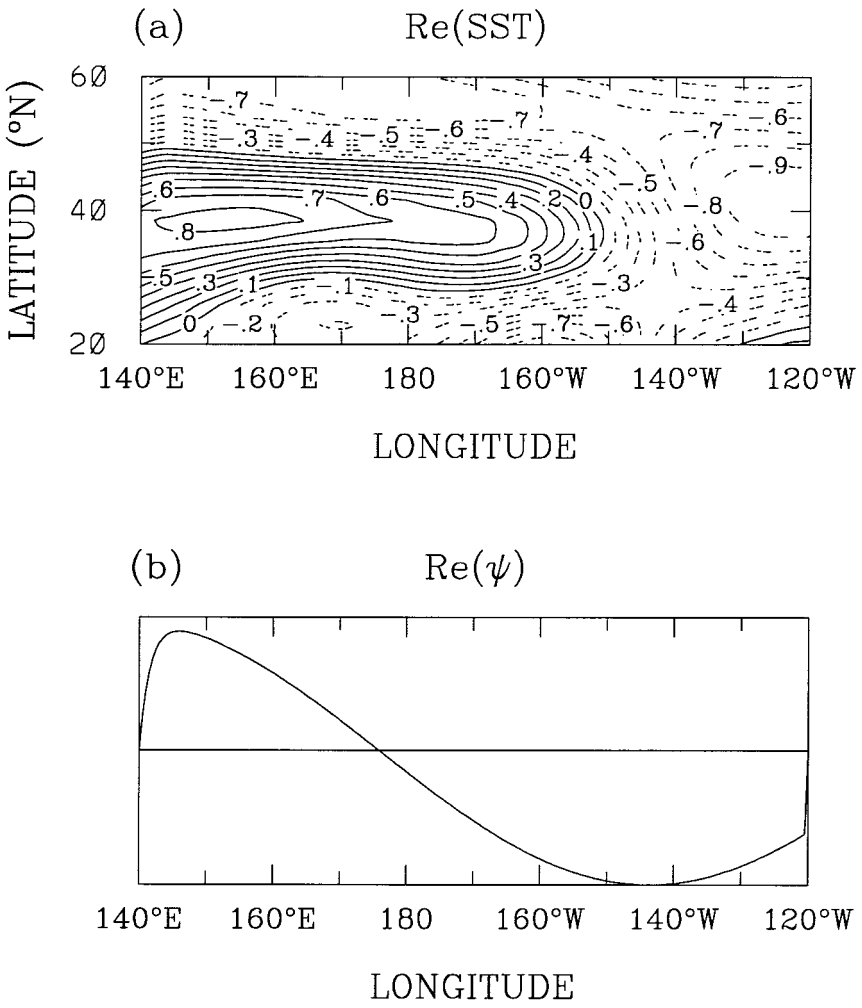

FIG. 8. Same as Fig. 4 except in the North Pacific for the Lau and Nath (1990) case.

small. However, when atmospheric wind stress and heat flux are large [such as the Latif and Barnett (1994) case], we find that (6.3) still holds for the SST mode. In this case, a direct calculation from (6.3) gives a growth rate of 7.7 yr^{-1}, which is basically the same as the numerical result obtained in section 5. This is because the positive heat flux feedback [term 2 in (6.3)], assisted by the Ekman feedback (term 3), overcome local decay.

b. The interdecadal mode

The approximation (6.2) holds if b_H is $O(10^{-1}\ yr^{-3})$ or less. From Eq. (3.21), this holds if frequency is of $O(10^{-1}\ yr^{-1})$. Using (3.8) and (3.22)–(3.25), (6.2) can be further simplified to

$$\sigma_{2,3} \approx \underbrace{-\frac{\epsilon_c K^2 + \nu K^4}{K^2 + \lambda^{-2}}}_{\text{term 1}} \pm \underbrace{i\overbrace{\frac{\beta k}{K^2 + \lambda^{-2}}}^{\text{dominant}}\left(1 + \frac{\mu a_1}{b_1 \beta k}\right)^{1/2}}_{\text{term 2}} + \underbrace{\frac{\mu a_1 \beta k}{2b_1^2 (K^2 + \lambda^{-2})^2}}_{\text{term 3}} + \underbrace{\frac{\mu a_2}{2b_1 (K^2 + \lambda^{-2})}\left(1 + \frac{\mu a_1}{b_1 \beta k}\right)^{-1/2}}_{\text{term 4}}, \tag{6.4}$$

where K^2 and b_1 are given by (3.7) and (3.22), respectively, and

$$a_1 = \langle \theta_1 \mathrm{Im}(V_P) \rangle + \langle \theta_1 \mathrm{Im}(V_H) \rangle \tag{6.5}$$

$$a_2 = \langle \theta_1 \mathrm{Re}(V_P) \rangle \pm \langle \theta_1 \mathrm{Re}(V_H) \rangle. \tag{6.6}$$

The real part of $\sigma_{2,3}$ is determined by terms 1, 3, and 4, while the imaginary part of $\sigma_{2,3}$ is determined by term 2. Here βk and $K^2 + \lambda^{-2}$ are of the orders of $10^{-4}\ yr^{-1}\ km^{-2}$ and $10^{-3}\ km^{-2}$, respectively. In both oceans, $\langle \theta_1 V_P \rangle$ is of the order of about $10^{-4}\ yr^{-2}\ km^{-2}$. Then $\langle \theta_1 \mathrm{Im}(V_P) \rangle / b_1 \beta k$ in term 2 may be comparable with 1 when $\mu = 1$. However, numerical results show that a_1 is of two orders of magnitude smaller than that of $\langle \theta_1 \mathrm{Im}(V_P) \rangle$ due to the cancellation of the two terms in a_1. Therefore, term 2 is dominated by $\beta k/(K^2 +$

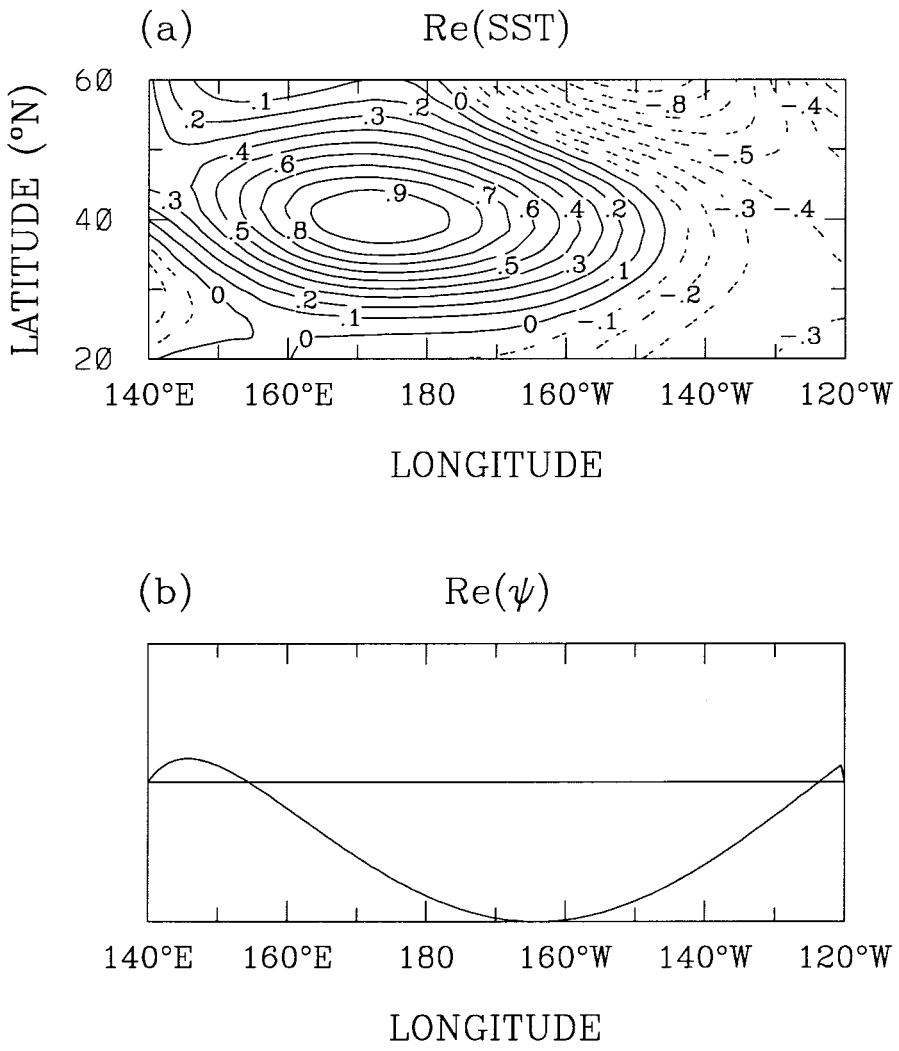

FIG. 9. Same as Fig. 4 except in the North Pacific for the Latif and Barnett-like case.

λ^{-2}), which is of the order of 10^{-1} yr^{-1} for both oceans. This term is familiar as the ocean baroclinic Rossby wave frequency for wavenumber k. Thus the bottom line of the analysis of the apparently complex coupled system is a very simple result for the interdecadal frequency. And yet the results in Fig. 3 argue strongly that coupling is essential to the interdecadal mode. The most important effects of coupling in (6.4) come from the fact that k is chosen by the atmospheric feedback. We underline that (6.4) does not hold as $\mu \to 0$, since dominance of the particular solution is assumed (see appendix C for a form suitable for examining low coupling cases).

For the decay rate, for example, when ϵ_c equals 1 yr^{-1} and ν equals 10^2 m^2 s^{-1}, term 1 is of the order of 10^{-3} yr^{-1}. Similarly, a_2 is two orders of magnitude smaller than $\langle \theta_1 \mathrm{Re}(V_P) \rangle$ due to the cancellation of the two terms in a_2. Then term 3 is of the order of 10^{-4} yr^{-1} or less and term 4 is less than about 10^{-3} yr^{-1}. In this case, the real part of the frequency is dominated by term 1, but term 4 also plays a role. Thus, the friction and diffusion terms in the vorticity equation cause the wave to decay, but the large spatial scales make the decay relatively slow.

Another consequence that may be drawn from (6.4) concerns the heat flux feedback. Both the local and nonlocal heat flux feedback effects are contained in b_1 [which is given by (3.22)]. The magnitude of the terms containing b_1, and the nature of the dependence, indicate that the heat flux feedback will not amplify the interdecadal mode. This differs, for instance, from the conjecture of Latif and Barnett (1994). The effect of the heat flux feedback is felt most directly in the SST mode as discussed above. On the slow, interdecadal timescales, the time derivative of SST is negligible, so the effect of the heat flux feedback on the interdecadal mode is on the pattern of SST anomalies, in a balance that also involves the advection of the

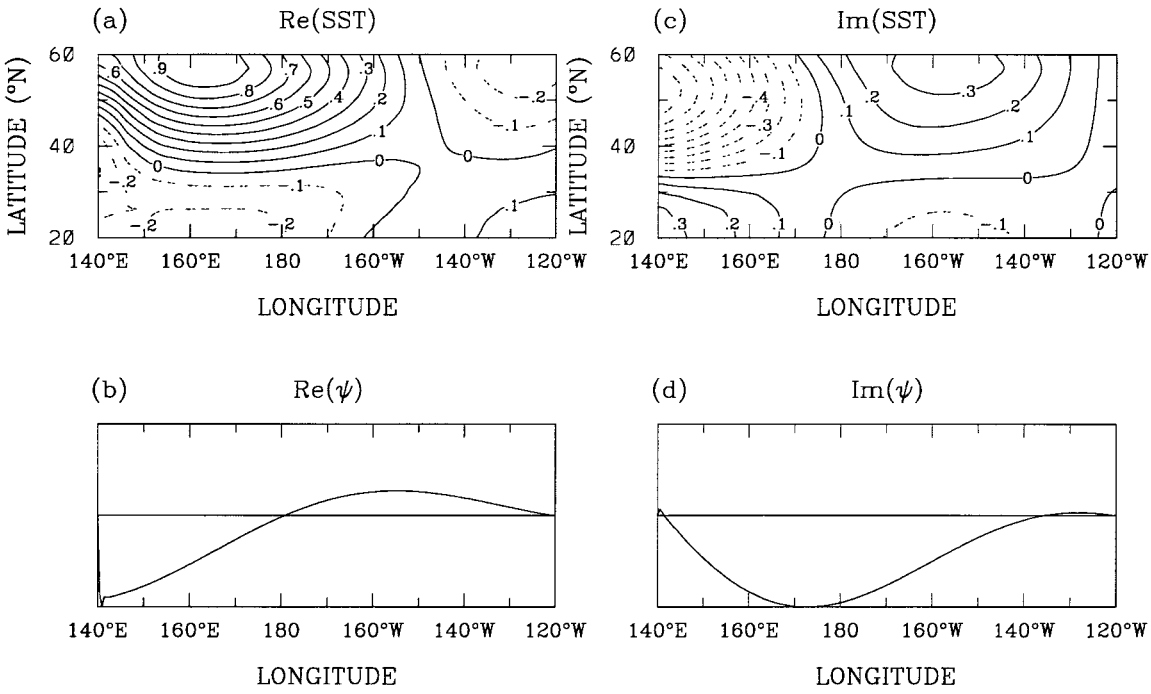

FIG. 10. Same as Fig. 5 except in the North Pacific for the Lau and Nath (1990) case.

climatological SST by the ocean currents. If the heat flux feedback is set to zero, the interdecadal mode still exists. Heat flux feedbacks thus modify the mode, but in a way that is very indirect; correlation of heat flux into the ocean with warm SST does not necessarily imply destabilization of the interdecadal mode.

Although (6.4) is obtained under the assumption that atmospheric wind stress and heat flux feedbacks are small, we test this expression for larger feedbacks, such as the Latif and Barnett (1994) case. We find that the interdecadal mode period is still dominated by $(K^2 + \lambda^{-2})/\beta k$. Since the main effect of the feedbacks is to choose the spatial scale, this continues to be true with the larger magnitude of the feedback. The timescale set by Rossby wave propagation remains the same.

For a simple case $\nu = 0$, the approximate analytic solution for $\tilde{\psi}(x)$ [see Weng (1997) for detailed derivation] is

$$\tilde{\psi}(x) \approx \frac{\mu l \tau_A \Lambda^2 \langle \theta_1 \tilde{T} \rangle}{2\rho H \sigma'} \times e^{\pm i\alpha}\{e^{\pm ikx}[e^{\epsilon_c K^2 (L_x - x)/\beta} - 1] + (1 - e^{\epsilon_c K^2 L_x/\beta}) e^{x(-\beta\epsilon_c \pm i\beta^2 k\lambda^2)/[\epsilon_c^2 + (\beta k\lambda^2)^2]}\}, \quad (6.7)$$

where

$$\sigma' = \sigma_{2,3} - \frac{\epsilon_c K^2 + \nu K^4}{K^2 + \lambda^{-2}} \pm i \frac{\beta k}{K^2 + \lambda^{-2}}. \quad (6.8)$$

From the above expression, the x dependence of the streamfunction is determined by the two terms in the curly bracket. The first term shows a sinusoid wave shape, which decays toward the east. Its length scale is set by the length scale of the wind stress feedback. The decay of the wave toward the east is caused by friction and β-effect. The second term matches the boundary condition $\tilde{\psi} = 0$ at the western boundary. In this approximate solution, $\tilde{\psi}(x)$ at the eastern boundary is not exactly zero but is very close.

7. Summary

Eigenvalue analysis is used to examine the modes of the simple ocean–atmosphere model whose response under stochastic forcing was analyzed in WN98 and NW99. The method of eigenvalue analysis used here may prove interesting for other systems involving nonlocal feedbacks: rather than brute force numerical methods, we first reduce the system analytically, taking inner products over the basin. Nonlocal feedbacks act via their inner product with the SST basis function with which they are associated.

Ocean basin modes in the uncoupled system have nearly continuous spectrum and no preferred structures, so none of these modes would be expected to stand out in a stochastically forced problem. Most of this spectrum is essentially unaffected by coupling. The SST modes found in both coupled and uncoupled systems are mainly affected by the heat flux feedback. The uncoupled SST mode decays purely with decay rate determined by

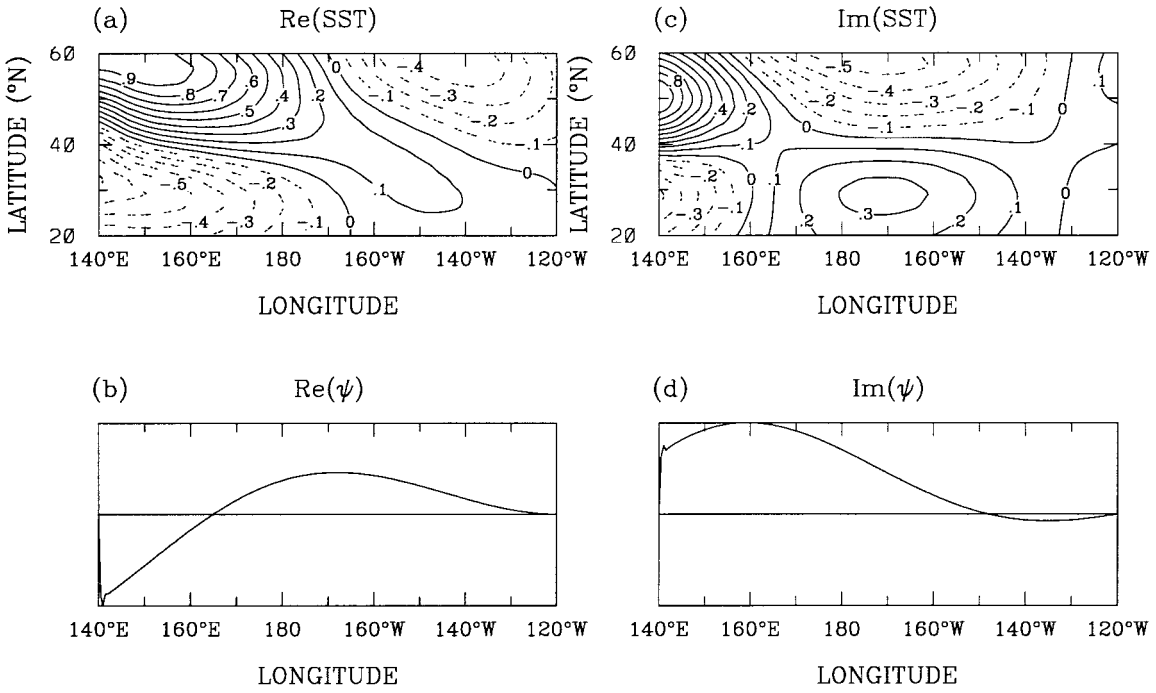

FIG. 11. Same as Fig. 5 except in the North Pacific for the Latif and Barnett-like case.

the local surface heat flux feedback. Coupling increases or decreases the decay rate of the corresponding uncoupled SST mode depending on whether the nonlocal heat flux feedback is negative or positive. The similarity between the nonlocal heat flux feedback and the spatial pattern of SST anomalies of the coupled SST mode provides the evidence of the dominant role of the heat flux in the SST mode. This mode is nonoscillatory. These results are consistent with those found in a stochastically forced case (NW99): heat flux plays an important role in generating SST anomalies whose power spectra is basically red, as in Hasselmann's (1976) hypothesis.

One interdecadal mode stands out distinctly. It is so strongly affected by coupling that it is qualitatively different from any mode in the uncoupled ocean spectrum. This is the most interesting mode not only because of its large spatial scale and its interdecadal timescale, but also because this mode is weakly decaying. The slow decay assists its maintenance by stochastic forcing from the atmosphere. The streamfunction of this mode propagates to the west and has a smooth large-scale pattern, which decays eastward due to the β-effect as balanced by the friction term. The large-scale north–south dipole pattern of the SST anomaly is generated by the advection of climatological SST by perturbation geostrophic currents. SST tends not to show westward propagation, since the basic state SST gradient is concentrated in the certain regions. Mechanisms of SST advection by mean currents (Sutton and Allen 1997; Latif and Barnett 1996) are not included here. Due to the longer zonal wavelength of the wind stress in the North Pacific than that in the North Atlantic, the period and zonal length scale of the interdecadal mode in the North Pacific are longer than that in the North Atlantic but not in proportion to the basin width. These features are similar to those found in the EOF and power spectral analyses of the time series obtained from integrating the model for the coupled case with small heat flux (NW99).

In NW99, we used time integration method to test the Latif and Barnett (1994) case in a stochastically forced system. Due to their large heat flux and wind stress feedbacks, SST anomalies grow exponentially with time. Here in the eigenvalue analysis, we are able to examine the interdecadal mode in this large-feedback case. The period and spatial structure of the mode are insensitive to the magnitude of the feedbacks. The SST mode can become unstable in this case but the interdecadal mode does not. We note that nonoscillatory instabilities such as that found for the SST mode are often by-products of flux-correction or anomaly modeling (Neelin and Dijkstra 1995), so we do not emphasize this case.

As shown by NW99 and WN98, the interdecadal mode can be excited by atmospheric stochastic wind stress forcing. The power spectrum of the stochastically forced case exhibits a reddened background spectrum, on top of which the interdecadal mode can appear as a spectral peak. Although the amplitude of the atmospheric feedback is weak compared to the

internal atmospheric variance, coupling plays an essential role in producing a mode whose signature is distinct from other modes in the system. The analytical results show how, despite the apparent complexity of matching ocean boundary conditions, and the seeming weakness of the atmospheric feedback, the imprint of the atmospheric spatial pattern nontheless emerges as an important constraint on the ocean Rossby wave dynamics. The feedback can thus set a preferred length scale and provide an eastward return mechanism to complement westward long Rossby wave propagation. The overall similarity of the modes found in the eigenvalue problem here provides confirmation that the leading EOFs and spectral peaks in the stochastically forced case are indeed associated with a well-defined large-scale interdecadal coupled mode of the system. This interdecadal mode is due to the dynamic interaction between the large-scale oceanic circulation and the atmosphere as suggested by Bjerknes (1964) and Kushnir (1994). Seeking such coupled interdecadal oscillations in observations, however, may be expected to be challenging, given that there is a large amount of variance associated with the red response of other modes to atmospheric stochastic forcing.

Acknowledgments. This work was supported by National Science Foundation Grant ATM-9521389. NCAR's Scientific Computing Division provided computer resources. We wish to thank Drs. M. Ghil, M. Latif, J. McWilliams, A. Robertson, and N. Schneider for their suggestions and comments.

APPENDIX A

Matching the Boundary Conditions on the Potential Vorticity Equation

The homogeneous solution, ψ_H, can be obtained by solving the differential equation (3.10) with the boundary conditions of (i) no flow across the boundary and (ii) a no-slip condition on the western and eastern boundaries. That is,

$$\psi_H(x) + \psi_P(x) = 0, \quad \text{for } x = 0, \text{ or } x = L_x \tag{A.1}$$

$$\partial_x[\psi_H(x) + \psi_P(x)] = 0, \quad \text{for } x = 0, \text{ or } x = L_x, \tag{A.2}$$

where $x = 0$ and $x = L_x$ correspond to the western and eastern boundaries, respectively. This gives

$$\psi_H(x) = \frac{\mu l \tau_A \langle \theta_1 \tilde{T} \rangle}{\rho H(A^2 + \beta^2 k^2)} \psi_h(x, \sigma), \tag{A.3}$$

where

$$\psi_h(x, \sigma) = c_1 e^{r_1 x} + c_2 e^{r_2 x} + c_3 e^{r_3 x} + c_4 e^{r_4 x}. \tag{A.4}$$

When the horizontal diffusion term is included, the four roots, r_1, r_2, r_3, and r_4, can be obtained numerically from

$$\nu r^4 - (2\nu l^2 + \sigma + \epsilon_c) r^2 - \beta r + \sigma(l^2 + \lambda^{-2}) + \nu l^4 + \epsilon_c l^2 = 0. \tag{A.5}$$

The four amplitudes c_1, c_2, c_3, and c_4 can be determined by the boundary conditions (i) and (ii). Note both the roots r_i and amplitudes c_i ($i = 1, 2, 3, 4$) depend on frequency.

Without the horizontal diffusion term (i.e., $\nu = 0$), (3.10) becomes a second-order differential equation. For a form similar to (A.3) (with $c_3 = c_4 = 0$), the two roots are

$$r_{1,2} = \frac{-\beta \pm \{\beta^2 + 4(\sigma + \epsilon_c)[\sigma(l^2 + \lambda^{-2}) + \epsilon_c l^2]\}^{1/2}}{2(\sigma + \epsilon_c)}. \tag{A.6}$$

Amplitudes c_1 and c_2 can be determined by boundary condition (i), which gives frequency dependent solutions

$$c_1 = A\frac{e^{r_2 L_x}\cos\alpha - \cos(kL_x + \alpha)}{e^{r_2 L_x} - e^{r_1 L_x}} - \beta k \frac{e^{r_2 L_x}\sin\alpha - \sin(kL_x + \alpha)}{e^{r_2 L_x} - e^{r_1 L_x}} \tag{A.7}$$

$$c_2 = A\frac{e^{r_1 L_x}\cos\alpha - \cos(kL_x + \alpha)}{e^{r_1 L_x} - e^{r_2 L_x}} - \beta k \frac{e^{r_1 L_x}\sin\alpha - \sin(kL_x + \alpha)}{e^{r_1 L_x} - e^{r_2 L_x}}. \tag{A.8}$$

APPENDIX B

Uncoupled Ocean Modes

When ($\mu = 0$), Eqs. (3.3) and (3.4) become the uncoupled ocean-only model in which the shallow water subsystem separates from the SST anomaly equation. There are two types of modes in this uncoupled system: the SST mode and the ocean basin mode, which can be obtained by solving the uncoupled ocean model with certain boundary conditions. Here we present the case when $\nu = 0$. The boundary condition used is no flow across the western and eastern boundaries.

The frequency of the SST mode can be obtained from SST equation and is

$$\sigma = -\epsilon_T. \tag{B.1}$$

The associated eigenvector is

$$\begin{cases} \tilde{\psi}(x) = 0, \\ \tilde{T}(x, y) = \text{arbitrary}. \end{cases} \tag{B.2}$$

The arbitrary spatial pattern is associated with a degenerate set of eigenmodes with the same frequency. This degeneracy can be broken by including diffusion, or by coupling.

Ocean basin mode solutions are known (e.g., Ped-

losky 1987), and are mainly discussed in the barotropic case. We provide solutions for the baroclinic case simply for reference. The frequency of the uncoupled ocean basin modes is

$$\sigma = -\epsilon_c + \frac{2\epsilon_c\lambda^{-2} \pm \{(2\epsilon_c\lambda^{-2})^2 - \beta^2[4(l^2 + \lambda^{-2}) + (2\pi n/L_x)^2]\}^{1/2}}{4(l^2 + \lambda^{-2}) + (2\pi n/L_x)^2}. \tag{B.3}$$

When n is small such that $\lambda^{-2} \gg (\pi n/L_x)^2$, (B.3) can be approximated by

$$\sigma \approx -\frac{\epsilon_c}{2} \pm i\frac{\beta}{2(l^2 + \lambda^{-2})^{1/2}}. \tag{B.4}$$

In this small limit, the decay rate is about $\epsilon_c/2$ and the frequency is about 9 yr^{-1}. This timescale is mainly determined by the β-effect and the Rossby deformation radius since l is much smaller than λ^{-1}.

When n is large such that $\lambda^{-2} \ll (\pi n/L_x)^2$, (B.3) can be approximated by

$$\sigma \approx -\epsilon_c \pm i\frac{\beta L_x}{2\pi n}, \tag{B.5}$$

which shows that the decay rate is about ϵ_c, and for given n, the frequency is determined by β-effect and the width of the ocean basin. As n goes to infinity, the frequency goes to 0.

The eigenvectors associated with the frequency given by (B.3) are

$$\tilde{\psi}(x) = 2e^{-\epsilon_c x/(\beta\lambda^2)} \sin\left(\frac{n\pi x}{L_x}\right) \times \left[\pm\sin\left(\frac{x}{D}\right) + i\cos\left(\frac{x}{D}\right)\right] \tag{B.6}$$

$$\tilde{T}(x, y) = \frac{\mathcal{L}[\tilde{\psi}(x)]}{\sigma + \epsilon_c}, \tag{B.7}$$

where $\mathcal{L}$ and σ are given by (3.14) and (B.3), respectively, and

$$D^{-1} = \sqrt{l^2 + \lambda^{-2} + (\pi n/L_x)^2 - (\epsilon_c\beta^{-1}\lambda^{-2})^2}. \tag{B.8}$$

When n is small, D is around 32 km. Here D decreases as n increases, and is real because λ^{-2} is greater than $(\epsilon_c\beta^{-1}\lambda^{-2})^2$.

APPENDIX C

Small Coupling Case

This appendix gives the solution form for the coupled frequency, suitable for taking the limit of small coupling. For a simple case $\nu = 0$,

$$\sigma = -\epsilon_c + \frac{2\epsilon_c\lambda^{-2} \pm \left\{(2\epsilon_c\lambda^{-2})^2 - \beta^2\left[4(l^2 + \lambda^{-2}) - \left(\frac{a(\sigma) + i2\pi n}{L_x}\right)^2\right]\right\}^{1/2}}{4(l^2 + \lambda^{-2}) - \left(\frac{a(\sigma) + i2\pi n}{L_x}\right)^2}, \tag{C.1}$$

where

$$a(\sigma) = \ln\left[\frac{(\sigma + \epsilon_T - \mu B)(A^2 + \beta^2k^2) - \mu\langle\theta_1V_p\rangle - \mu\langle\theta_1V_{h2}\rangle}{(\sigma + \epsilon_T - \mu B)(A^2 + \beta^2k^2) - \mu\langle\theta_1V_p\rangle - \mu\langle\theta_1V_{h1}\rangle}\right] \tag{C.2}$$

$$B = \langle\theta_1Q_{\text{FB}}\rangle + \langle\theta_1V_E\rangle \tag{C.3}$$

$$V_p = \frac{l\tau_A}{\rho H}\mathcal{L}[\beta k\sin(kx + \alpha) - A\cos(kx + \alpha)] \tag{C.4}$$

$$V_{h1} = \frac{l\tau_A}{\rho H}\mathcal{L}\{(A\cos\alpha - \beta k\sin\alpha)e^{r_2x} + [A\cos(kL_x + \alpha) - \beta k\sin(kL_x + \alpha)]e^{r_1(x-L_x)}\} \tag{C.5}$$

$$V_{h2} = \frac{l\tau_A}{\rho H}\mathcal{L}\{(A\cos\alpha - \beta k\sin\alpha)e^{r_1x} + [A\cos(kL_x + \alpha) - \beta k\sin(kL_x + \alpha)]e^{r_2(x-L_x)}\} \tag{C.6}$$

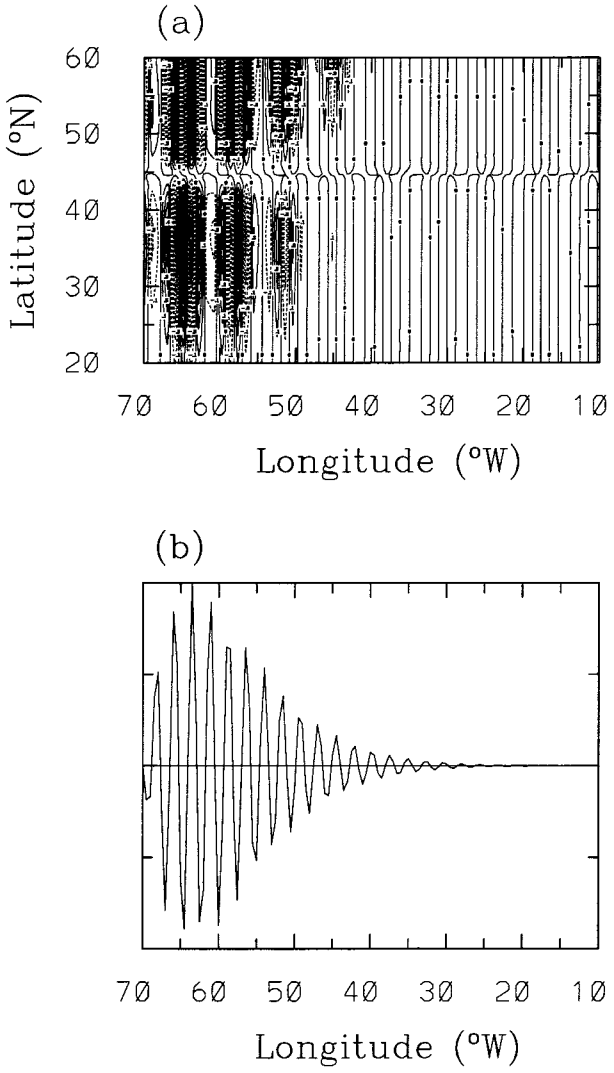

FIG. C1. (a) The spatial distribution of the SST anomaly, and (b) the zonal dependence of the streamfunction in the North Atlantic Ocean for the gravest ocean basin mode ($n = \pm 1$).

and $\mathcal{L}$ is given by (3.14). Here r_1 and r_2 are given by Eq. (A.6), A is given by Eq. (3.6), and A, r_1, r_2, $\langle \theta_1 V_{h1} \rangle$, and $\langle \theta_1 V_{h2} \rangle$ are functions of frequency.

In the limit μ goes to zero, $a(\sigma)$ goes to zero. In this limit, (C.1) is the same as (B.3), which is for the uncoupled ocean basin modes. For the standard coupling case ($\mu = 1$), $a(\sigma)$ is much less than 1 for the ocean basin modes shown in Fig. 3. Therefore, (C.1) with $a \approx 0$ gives the approximate frequency for the coupled ocean basin modes. Consequently, their spatial structures of $\tilde{\psi}(x)$ and $\tilde{T}(x, y)$ are similar to that of the corresponding uncoupled modes. Figure C1 shows $\tilde{\psi}(x)$ and $\tilde{T}(x, y)$ for $n = 1$, which are very similar to the eigenvectors of the corresponding uncoupled mode given in (B.6) and (B.7), respectively.

The interdecadal mode is in principal also contained in (C.1)–(C.2), for the case $\nu = 0$, although in practice this form appears numerically impractical. However, the differences between (C.1) and the approximation (6.4) that gives the dominant behavior of the interdecadal mode illustrate the subtlety of the transition to low coupling. Letting $\mu \to 0$ in (6.4) gives incorrect results because the coupling terms have been assumed not to be small. In (C.2), letting $\mu \to 0$ gives $a(\sigma) \to \ln(1) = 0$ so (C.1) results in ocean basin modes. If μ is not small, then when

$$A^2 + \beta^2 k^2 \approx 0, \tag{C.7}$$

$a(\sigma)$ can be large when $\langle \theta_1 V_{h2} \rangle$ differs sufficiently from $\langle \theta_1 V_{h1} \rangle$. Since (C.7) gives the interdecadal frequency by the Rossby-like dispersion relation, and small σ gives r_1 and r_2 very different, $\langle \theta_1 V_{h2} \rangle$ in fact differs from $\langle \theta_1 V_{h1} \rangle$ by many orders of magnitude (and hence produces numerical problems in finding the interdecadal mode). Physically, what this process illustrates is that the importance of the coupling must be measured via its effect on ocean spatial structures, rather than by comparison to atmospheric uncoupled variability.

REFERENCES

Battisti, D. S., U. S. Bhatt, and M. A. Alexander, 1995: A modeling study of the interannual variability in the North Atlantic Ocean. *J. Climate*, **8,** 3067–3083.

Bjerknes, J., 1962: Synoptic survey of the interaction between sea and atmosphere in the North Atlantic. *Geophys. Publ.*, **24,** 116–145.

——, 1964: Atlantic air–sea interaction. *Advances in Geophysics*, Vol. 10, Academic Press, 1–82.

Chen, F., and M. Ghil, 1995: Interdecadal variability of the thermohaline circulation and high-latitude surface fluxes. *J. Phys. Oceanogr.*, **25,** 2547–2568.

Delworth, T., S. Manabe, and R. J. Stouffer, 1993: Interdecadal variations of the thermohaline circulation in a coupled ocean–atmosphere model. *J. Climate*, **6,** 1993–2011.

Deser, C., and M. L. Blackmon, 1993: Surface climate variations over the North Atlantic Ocean during winter: 1900–1989. *J. Climate*, **6,** 1743–1753.

Ferranti, L., F. Molteni, and T. N. Palmer, 1994: Impact of localized tropical and extratropical SST anomalies in ensembles of seasonal GCM integrations. *Quart. J. Roy. Meteor. Soc.*, **120,** 1613–1645.

Folland, C. K., and D. Parker, 1989: Observed variations of sea surface temperature. *Proc. NATO Advanced Research Workshop on Climate Ocean Interaction*, Kluwer Academic Press.

Frankignoul, C., and K. Hasselmann, 1977: Stochastic climate models, Part II: Application to sea-surface temperature variability and thermocline variability. *Tellus*, **29,** 289–305.

——, P. Muller, and E. Zorita, 1997: A simple model of the decadal response of the ocean to stochastic wind forcing. *J. Phys. Oceanogr.*, **27,** 1533–1546.

Graham, N. E., 1994: Decadal-scale climate variability in the tropical and North Pacific during the 1970s and 1980s: Observations and model results. *Climate Dyn.*, **10,** 135–162.

——, T. P. Barnett, R. Wilde, M. Ponater, and S. Schubert, 1994: On the roles of tropical and midlatitude SSTs in forcing interannual to interdecadal variability in the winter Northern Hemisphere circulation. *J. Climate*, **7,** 1416–1441.

Grötzner, A., M. Latif, and T. P. Barnett, 1998: A decadal climate cycle in the North Atlantic 2, ocean as simulated by the ECHO coupled GCM. *J. Climate*, **11,** 831–847.

Hasselmann, K., 1976: Stochastic climate models. Part I: Theory. *Tellus,* **28,** 289–305.

Jin, F.-F., 1997: A theory of interdecadal climate variability of the North Pacific ocean–atmosphere system. *J. Climate,* **10,** 324–338.

Kharin, V. V., 1995: The relationship between sea surface temperature anomalies and atmospheric circulation in GCM experiments. *Climate Dyn.,* **11,** 359–375.

Kushnir, Y., 1994: Interdecadal variations in North Atlantic sea surface temperature and associated atmospheric conditions. *J. Climate,* **7,** 141–157.

——, and N. C. Lau, 1992: The general circulation model response to a North Pacific SST anomaly: Dependence on time scale and pattern polarity. *J. Climate,* **5,** 271–283.

Latif, M., 1998: Dynamics of interdecadal variability in coupled ocean–atmosphere models. *J. Climate,* **11,** 602–624.

——, and T. P. Barnett, 1994: Causes of decadal climate variability in the North Pacific/North American sector. *Science,* **266,** 634–637.

——, and ——, 1996: Decadal climate variability over the North Pacific and North America: Dynamics and predictability. *J. Climate,* **9,** 2407–2423.

Lau, N. C., and M. J. Nath, 1990: A general circulation model study of the atmospheric response to extratropical SST anomalies observed during 1950–79. *J. Climate,* **3,** 965–989.

Liu, Z., 1993: Interannual positive feedback in a simple extratropical air–sea coupling system. *J. Atmos. Sci.,* **50,** 3022–3028.

Münnich, M., M. Latif, S. Venzke, and E. Maier-Reimer, 1998: Decadal oscillations in a simple coupled model. *J. Climate,* **11,** 3309–3319.

Namias, J., and D. R. Cayan, 1981: Large-scale air–sea interactions and short period climate fluctuations. *Science,* **214,** 869–876.

Neelin, J. D., and H. A. Dijkstra, 1995: Ocean–atmosphere interaction and the tropical climatology. Part I: The dangers of flux correction. *J. Climate,* **8,** 1325–1342.

——, and W. Weng, 1999: Analytical prototypes for ocean–atmosphere interaction at midlatitudes. Part I: Coupled feedbacks as a sea surface temperature dependent stochastic process. *J. Climate,* **12,** 697–721.

Palmer, T. N., and Z. Sun, 1985: A modeling and observational study of the relationship between sea surface temperature in the northwest Atlantic and the atmospheric general circulation. *Quart. J. Roy. Meteor. Soc.,* **111,** 947–975.

Pedlosky, J., 1987: *Geophysical Fluid Dynamics.* 2d ed. Springer-Verlag, 710 pp.

Peng, S., L. A. Mysak, H. Ritchie, J. Derome, and B. Dugas, 1995: The difference between early and middle winter atmospheric response to sea surface temperature anomalies in the northwest Atlantic. *J. Climate,* **8,** 137–157.

Robertson, A. W., 1996: Interdecadal variability over the North Pacific in a multi-century climate simulation. *Climate Dyn.,* **12,** 227–241.

Saravanan, R., and J. C. McWilliams, 1997: Stochasticity and spatial resonance in interdecadal climate fluctuations. *J. Climate,* **10,** 2299–2320.

Selten, F. M., R. J. Haarsma, and J. D. Opsteegh, 1999: On the mechanism of North Atlantic decadal variability. *J. Climate,* **12,** 1956–1973.

Spall, M. A., 1996: Dynamics of the Gulf Stream/deep western boundary current crossover. Part II: Low-frequency internal oscillations. *J. Phys. Oceanogr.,* **26,** 2169–2182.

Speich, S., H. Dijkstra, and M. Ghil, 1995: Successive bifurcations in a shallow-water model applied to the wind-driven ocean circulation. *Nonlin. Proc. Geophys.,* **2,** 241–268.

Sutton, R. T., and M. R. Allen, 1997: Decadal predictability of North Atlantic sea surface temperature and climate. *Nature,* **388,** 563–567.

Trenberth, K. E., 1990: Recent observed interdecadal climate changes in the Northern Hemisphere. *Bull. Amer. Meteor. Soc.,* **71,** 988–993.

——, and J. Hurrell, 1994: Decadal atmosphere–ocean variations in the Pacific. *Climate Dyn.,* **9,** 303–319.

von Storch, J. S., 1994: Interdecadal variability in a global coupled model. *Tellus,* **46A,** 419–436.

Wallace, J. M., C. Smith, and Q. Jiang, 1990: Spatial patterns of atmosphere–ocean interaction in the northern winter. *J. Climate,* **3,** 990–998.

Weaver, A. J., E. S. Sarachik, and J. Marotze, 1991: Freshwater flux forcing of decadal and interdecadal oceanic variability. *Nature,* **353,** 836–838.

——, S. M. Aura, and P. G. Myers, 1994: Interdecadal variability in an idealized model of the North Atlantic. *J. Geophys. Res.,* **99,** 12 423–12 441.

Weng, W., 1997: A simple model for ocean–atmosphere interaction at midlatitudes. Ph.D. dissertation, University of California, Los Angeles, 128 pp. [Available from University Microfilm, 305 N. Zeeb Rd., Ann Arbor, MI 48106.]

——, and J. D. Neelin, 1998: On the role of ocean–atmosphere interaction in midlatitude interdecadal variability. *Geophys. Res. Letter,* **25,** 167–170.

Zorita, E., and C. Frankignoul, 1997: Modes of North Atlantic decadal variability in the ECHAM1/LSG coupled ocean–atmosphere general circulation model. *J. Climate,* **10,** 183–200.

——, V. Kharin, and H. von Storch, 1992: The atmospheric circulation and sea surface temperature in the North Atlantic area in Winter: Their interaction and relevance for Iberian precipitation. *J. Climate,* **5,** 1097–1108.